

1 Investigation of An Extreme Rainfall Event during 8-12 December 2018 over

2 Central Vietnam. Part I: Analysis and Cloud-Resolving Simulation

4 Chung-Chieh Wang and Duc Van Nguyen*

6 Department of Earth Sciences, National Taiwan Normal University, Taipei, Taiwan

8 Corresponding author address: Duc Van Nguyen (nguyenvanduc_t57@hus.edu.vn),
9 Department of Earth Sciences, National Taiwan Normal University, No. 88, Sec. 4, Ting-
10 Chou Rd., Taipei 11677, Taiwan

11 Highlights:

- A record-breaking rainfall event over central Vietnam is investigated and its simulation result using a cloud resolving model is evaluated
- Key factors in this event include the combined effect of northeasterly wind that originated from northern China, low-level easterly wind blow to central Vietnam from the northwest Pacific Ocean, southeasterly wind, local topography, and high sea surface temperature over North West Pacific ocean and South China Sea.
- A cloud-resolving model is applied to simulated this study an extreme rainfall event in central Vietnam, and the results show that the model mostly captured the quantitative rainfall of this event. These results are very impressive.

Formatted: Font color: Green

21

Abstract

22 An extreme rainfall event occurred from 8 to 12 December 2018 along the coast of central
 23 Vietnam. The observed maximum rainfall amount in 72 h was over 900 mm and set a new record,
 24 and the associated heavy losses were also significant. The analysis of this event shows some key
 25 factors for its occurrence: (1) The interaction between the strong northeasterly winds, blowing from
 26 the Yellow Sea into the northern South China Sea (SCS), and easterly winds over the SCS in the
 27 lower troposphere (below 700 hPa). This interaction created strong low-level convergence, as the
 28 winds continued to blow into central Vietnam against the Truong Son Range, resulting in forced
 29 uplift over the coastal plains due to the terrain's barrier effect. Furthermore, the low-level
 30 convergence in this event was strong enough, and the air was unstable enough to trigger most of the
 31 convection near the shoreline (further inland). As a consequence, heavy rainfall occurred along the
 32 coastal zone and coastal sea. (2) The strong easterly wind played an important role in transporting
 33 moisture from the western North Pacific across the Philippines and the SCS into central Vietnam.
 34 (3) The Truong Son Range also contributed to this event due to its barrier effect. (4) In addition to
 35 cumulonimbus, the low-level precipitating clouds such as nimbostratus clouds were also major
 36 contributors to rainfall accumulation for the whole event. The analyses of local thermodynamics
 37 also indicate that the southward movement of the low-level wind convergence zone caused the
 38 southward movement of the main heavy rain band during the event.
 39 The Cloud-Resolving Storm Simulator (CReSS) was employed to simulate this record-
 40 breaking event at high resolution, and evaluated results show the model had good simulated the
 41 surface wind as well as captured the southward movement of the low-level wind convergence. The
 42 overall rainfall can be captured quite well not only in quantity but also in its spatial distribution
 43 (with a Fractions Skill Score ≈ 0.7 and Threat Score > 0 at 700 mm for 72 h rainfall). Thus, the
 44 CReSS model is shown to be a useful tool for both research and forecasts of heavy rainfall in
 45 Vietnam. The model performed better for the rainfall during 9-10 but not as good on 11 December.

← Formatted: Indent: First line: 0.31", Space After: 0 pt

Formatted: Font color: Green

Formatted: Font: (Default) Times New Roman, Font color: Green

Formatted: Font: (Default) Times New Roman, Font color: Green

Formatted: Font: (Default) Times New Roman, Font color: Green

Formatted: Font: (Default) Times New Roman

← Formatted: Indent: First line: 0.31"

Formatted: Font color: Green

46 In the sensitivity test without the terrain, the model had poorly simulated the surface wind, which
47 led-to the model did not generate nearly as much rainfall for this event. Thus, the test confirms the
48 important role played by the local topography for the occurrence of this event.

Formatted: Font color: Green

49 Keywords: Extreme rainfall, central Vietnam, cloud-resolving model.

50

51 1 Introduction

52 Heavy to extreme rainfalls are natural disasters that often cause deaths, flooding, landslides,
53 and erosion. Vietnam is one of the most disaster-prone countries in the world with many different
54 types of natural hazards disasters. In the country, central Vietnam is most affected by natural
55 disasters and climate change, with frequent occurrences of rainstorms and extreme rainfalls. For
56 example, during 8-12 December 2018, an extreme rainfall event (hereafter abbreviated as the D18
57 event) occurred along the coast of central Vietnam. The peak 72-h accumulated rainfall (from 1200
58 UTC 8 to 1200 UTC 11 Dec) at some stations exceeds 800 mm (Fig. 1d). Among the stations, Da
59 Nang (16.0° N, 108.2° E, cf. Figs. 1a,b) recorded 24-h rainfall amounts greater than 600 mm on 9
60 December and over 300 mm the next day. This extreme event resulted in 13 deaths, an estimated
61 1200 houses inundated, around 12,000 hectares of crops destroyed, some 160,000 livestock killed
62 and many other economic losses (Tuoi Tre news, 2018). Furthermore, according to a publication by
63 the Ministry of Natural Resources and Environment of Vietnam (Tran et al., 2016) regarding
64 climate change and sea-level rise scenarios climate change and sea level rise scenarios for Vietnam,
65 extreme precipitation events will increase in both their frequency and intensity in the future (Tran et
66 al., 2016). Hence, how to improve the ability in the quantitative precipitation forecast (QPF) of
67 heavy-rainfall events over central Vietnam is very important.

Formatted: Font color: Green

Formatted: Font: (Default) Times New Roman, 12 pt,
Font color: Green

Formatted: Font color: Green

Formatted: Font color: Green

Formatted: Font: (Default) Times New Roman, 12 pt,
Font color: Green

68 Climatologically, the central part of Vietnam is the country's rainiest region and is strongly
69 affected by heavy to extreme rainfall, with average annual precipitation ranging from 2400 to over

Formatted: Font color: Green

70 3300 mm (1980–2010, Fig. 1f). The main rainy season in this region is from late fall to early winter
71 (Yokoi and Matsumoto, 2008; Chen *et al.*, 2012). Past studies have shown some main factors that
72 can lead to heavy rainfall in central Vietnam, such as (1) the combined effect of cold surges that
73 originate from northern China, (2) tropical depressions, and (3) local topography due to the
74 topography is characterized by high mountains (< 3000 m), highlands, narrow coastal plain with the
75 narrowest place less than 100 km in width (east-west), and gradually lowers from the west to the
76 east (Fig. 1a) (Bui, 2019; Yokoi and Matsumoto, 2008; Chen *et al.*, 2012; Nguyen-Le and
77 Matsumoto, 2016; van der Linden *et al.*, 2016). According to these studies, a cool, dry continental
78 surface high pressure system (known as the Siberian high-pressure system) gradually establishes
79 over the continental East Asia after boreal summer in October–November. This high-pressure
80 system's intensification and southeastward amplification lead to an episodic southward progression
81 of cold surge into the tropics. The interaction of this cold surge and preexisting tropical disturbance
82 over the SCS and the topography in central Vietnam can bring large amounts of rainfall along the
83 east-central coast through orographic rainfall processes.

84 In this study, central Vietnam is referred to as the area between 14.7° N and 18° N (Fig. 2a). Its
85 eastern boundary is the South China Sea (SCS), and the western boundary is the border to Laos,
86 where the Truong Son Range (also known as the Annamite Range) runs parallel to the coast. The
87 central Vietnam includes Quang Binh, Quang Tri, Thua Thien Hue, Da Nang city, Quang Nam, and
88 a part of Quang Ngai province. The topography is characterized by high mountains (< 3000 m),
89 highlands, narrow coastal plain with the narrowest place less than 100 km in width (east-west), and
90 gradually lowers from the west to the east (Fig. 2b). Most of the population and cities are
91 concentrated along the coastal plain. By these characteristics of steep topography, when heavy rain
92 occurs, it often leads to flooding and causes great damages to people and the environment.

93

Formatted: Font color: Green

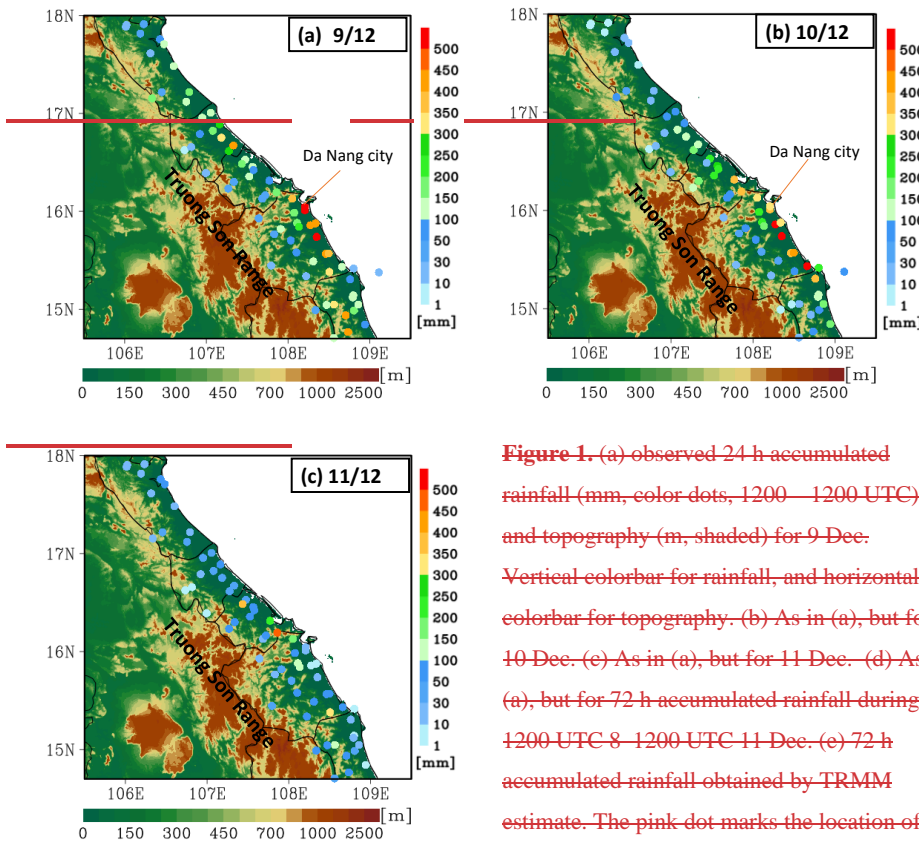
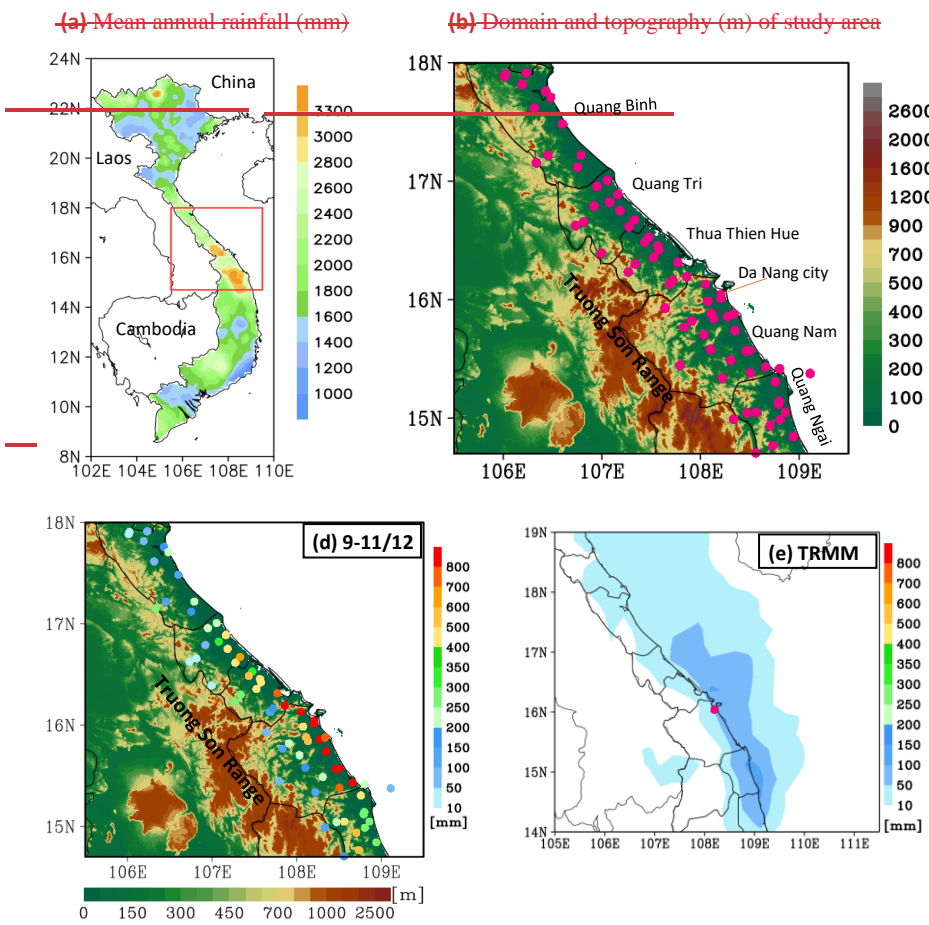


Figure 1. (a) observed 24 h accumulated rainfall (mm, color dots, 1200–1200 UTC) and topography (m, shaded) for 9 Dec. Vertical colorbar for rainfall, and horizontal colorbar for topography. (b) As in (a), but for 10 Dec. (c) As in (a), but for 11 Dec. (d) As in (a), but for 72 h accumulated rainfall during 1200 UTC 8–1200 UTC 11 Dec. (e) 72 h accumulated rainfall obtained by TRMM estimate. The pink dot marks the location of Da Nang station.

Formatted Table

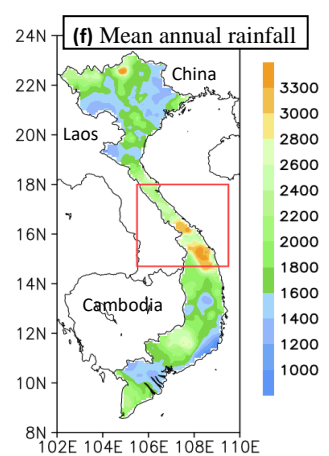
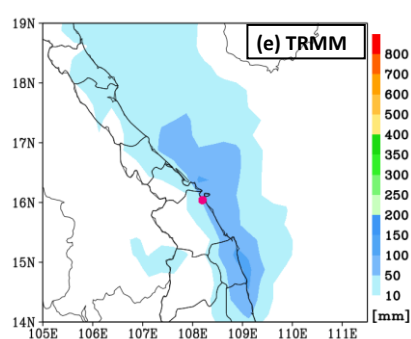
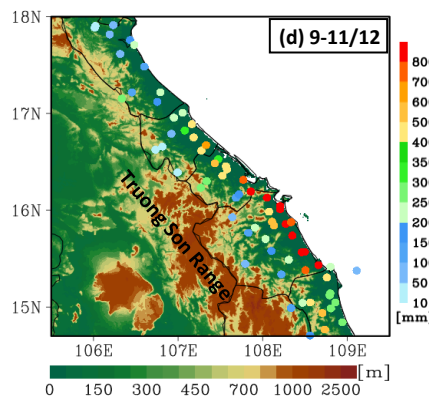
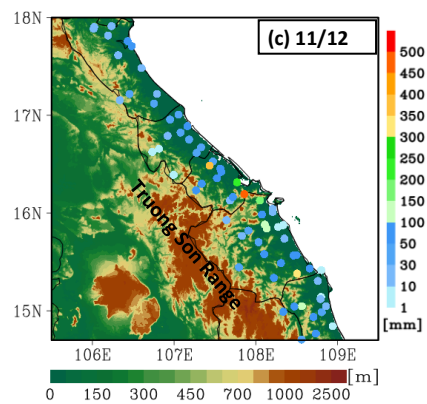
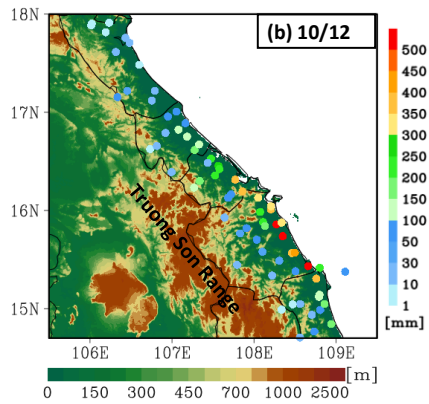
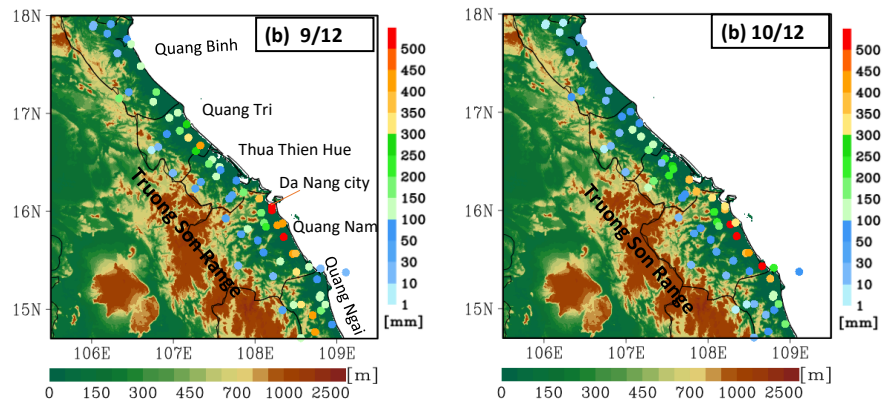


94 **Figure 2.** (a) Mean annual rainfall distribution (mm) in Vietnam from 1980 to 2010, obtained from
 95 the Vietnam Gridded Precipitation (VnGP) data, and the study area of central Vietnam (red box).
 96 (b) The domain and topography (m) of central Vietnam. Pink dots mark the locations of rain gauge
 97 stations.

98 Climatologically, the central part of Vietnam is the country's rainiest region and is strongly
99 affected by heavy to extreme rainfall, with average annual precipitation ranging from 2400 to over
100 3300 mm (1980–2010, Fig. 2a). The main rainy season in this region is from late fall to early winter
101 (Yokoi and Matsumoto, 2008; Chen *et al.*, 2012).

102 Past studies have shown some main factors that can lead to heavy rainfall in central Vietnam,
103 such as (1) the combined effect of cold surges that originate from northern China, (2) tropical
104 depressions, and (3) local topography (Bui, 2019; Yokoi and Matsumoto, 2008; Chen *et al.*, 2012;
105 Nguyen Le and Matsumoto, 2016; van der Linden *et al.*, 2016). According to these studies, a cool,
106 dry continental surface high pressure system (known as the Siberian high pressure system)
107 gradually establishes over the continental East Asia after boreal summer in October–November.
108 This high pressure system's intensification and southeastward amplification lead to an episodic
109 southward progression of cold surge into the tropics. The interaction of this cold surge and
110 preexisting tropical disturbance over the SCS and the topography in central Vietnam can bring large
111 amounts of rainfall along the east central coast through orographic rainfall processes.

112
113
114
115
116
117
118
119
120



121 [Figure 1.](#) (a) observed 24 h accumulated rainfall (mm, color dots, 1200 – 1200 UTC) and
122 topography (m, shaded) for 9 Dec. Vertical colorbar for rainfall, and horizontal colorbar for
123 topography. (b) As in (a), but for 10 Dec. (c) As in (a), but for 11 Dec. (d) As in (a), but for 72 h
124 accumulated rainfall during 1200 UTC 8–1200 UTC 11 Dec. (e) 72 h accumulated rainfall obtained
125 by TRMM estimate. The pink dot marks the location of Da Nang station. (f) Mean annual rainfall
126 distribution (mm) in Vietnam from 1980 to 2010, obtained from the Vietnam Gridded Precipitation
127 (VnGP) data, and the study area of central Vietnam (red box).

Formatted: Font: 12 pt, Font color: Green

128 Furthermore, According to Wang et al. (2017), Vietnam is impacted by about 4-6 typhoons
129 per year. Nguyen-Thi et al. (2012) investigated the characteristic of tropical cyclone rainfall over
130 Vietnam in the climatology. Their results show that the tropical cyclone rainfall amount is
131 concentrated in central Vietnam, peaking between October and November. Takahashi et al. (2009)
132 performed a long-term simulation for September (from 1966 to 1995) using a high-resolution
133 model. They found that the observed long-term decrease in September rainfall is due to the
134 weakening of tropical cyclone activity over the Indochina Peninsula. As for the impacts of El Niño-
135 Southern Oscillation (ENSO), some studies have examined the linkages between rainfall in
136 Vietnam and ENSO, and suggested more (less) rainfall during La Niña (El Niño) years. For
137 example, Yen et al. (2010) analyzed the interannual variation of the rainfall in fall over central
138 Vietnam, and their results indicated a negatively correlated relationship between rainfall in central
139 Vietnam and the sea surface temperature over the NINO3.4 region. Besides, Vu et al. (2015)
140 investigated the effects of ENSO on fall rainfall in central Vietnam and concluded that central
141 Vietnam has more (less) rainfall in La Niña (El Niño) years. Finally, Wu et al. (2012) analyzed the
142 Madden-Julian Oscillation (MJO) activity from September to November for 30 years (1981-2010)
143 over Vietnam and showed that the MJO is also an important factor in the formation of extreme
144 precipitation events in central Vietnam.

Formatted: Font color: Green

145 In recent decades, the Cloud-Resolving Storm Simulator (CReSS) has been widely known due
146 to its good performance in quantitative precipitation forecasts. This model has been applied to study
147 tropical cyclones, heavy to extreme rainfall events, and many other convective systems in Japan and

148 Taiwan (e.g., Ohigashi and Tsuboki, 2007; Yamada *et al.*, 2007; Akter and Tsuboki, 2010, 2012;
149 Wang *et al.*, 2015). Furthermore, the CReSS model has been used to perform routine high-
150 resolution forecasts at the National Taiwan Normal University (NTNU) and provided to the TTFRI
151 as a forecast member since 2010. Hence, this study employed the CReSS model to simulate the
152 D18 event and evaluated its performance.

Formatted: Font color: Green

153 From the review above, the important mechanisms for the heavy rainfall in some previous
154 events over central Vietnam are revealed. However, ~~the D18 event set a new historical rainfall~~
155 ~~record and left with heavy losses in central Vietnam. As the magnitude of the D18 event surpassed~~
156 ~~all past events according to Dr. Hoang Phuc Lam – National Center for Hydro- Meteorological~~
157 ~~Forecasting, it can be said that this extreme event has never happened in the past because the~~
158 ~~observed rainfall at some places in the Central region has surpassed the record according to the~~
159 ~~statistics of rainfall at the end of the main rainy season (Communist Party of Vietnam Online~~
160 ~~Newspaper), several questions are therefore raised: What mechanisms caused this record-breaking~~
161 ~~event at such a magnitude? Was its mechanism similar to those in previous events? Or, it was a~~
162 ~~different one. How important was the role played by local terrain in this event? From a forecast~~
163 ~~perspective, one related question would be whether a cloud-resolving ~~or high resolution~~ model is~~
164 ~~capable of reproducing the D18 event? The answers to these questions will help improve our~~
165 ~~understanding on the mechanisms that cause heavy rainfall in central Vietnam, as well as on the~~
166 ~~predictability of such events in the future. Hence, the present study was carried out with an aim to~~
167 ~~answer the above questions. The remainder of this paper is organized as follows: Section 2~~
168 ~~describes the datasets and methodology used in the study. The analysis and modeling results are~~
169 ~~presented in Section 3 and 4, respectively. Finally, the conclusions are given in Section 5.~~

Formatted: Font: (Default) Times New Roman, 12 pt,
Font color: Green

Formatted: Font: (Default) Times New Roman, 12 pt

Formatted: Font: (Default) Times New Roman, 12 pt,
Font color: Green

170 2 Data and Methodology

171 2.1 Data

172 2.1.1 NCEP GDAS/FNL Global Gridded Analyses and Forecasts

173 This dataset, [The NCEP GDAS/FNL Global Gridded Analyses and Forecasts](#), is provided freely
174 by the National Centers for Environmental Prediction (NCEP). In this study, this dataset is used as
175 the initial and boundary conditions (IC/BCs) for the cloud-resolving model (CRM) simulation. The
176 data are on a $0.25^\circ \times 0.25^\circ$ latitude-longitude grid with 26 levels extending from the surface to 20
177 hPa. The data period is from 0600 UTC 8 December to 0000 UTC 13 December 2018, at 6-h
178 intervals. Parameters include geopotential height, zonal and meridional wind components, pressure,
179 temperature, and relative humidity. The dataset and its detailed information are available at
180 <https://rda.ucar.edu/datasets/ds083.3>.

Formatted: Font: 12 pt, Font color: Green

Formatted: Font color: Green

181 2.1.2 The fifth generation ECMWF reanalysis data (ERA5)

182 The ERA5 is the fifth-generation reanalysis dataset, developed by the European Centre for
183 Medium-range Weather Forecasts (ECMWF) to replaces the ERA-Interim reanalysis. We have used
184 these data to delineate the synoptic weather patterns during the D18 event. The horizontal resolution
185 of this dataset is $0.25^\circ \times 0.25^\circ$ latitude-longitude at 22 selected levels from 1000 to 100 hPa and
186 including the surface. Parameters include zonal and meridional wind components, geopotential
187 height, specific humidity, relative humidity, temperature, vertical velocity, mean sea level pressure,
188 and sea surface temperature. The dataset was downloaded from 0000 UTC 8 to 1800 UTC 11
189 December 2018 at 6-h intervals ([Hersbach et al., 2018a,b](#)).

190 2.1.3 Observation data

191 The daily observed rainfall data (1200–1200 UTC, i.e., 1900–1900 LST) from 8 to 12
192 December 2018 at 69 automated gauge stations across central Vietnam are used for case overview
193 and verification of model results. This dataset is provided by the Mid-central Regional Hydro-
194 Meteorological Centre, Vietnam.

195 2.1.4 Satellite data

196 (a) TRMM (TMPA) rainfall estimates

197 The TRMM multi-satellite precipitation estimates (3B42, version 7, [Huffman *et al.*, 2016](#)) are
198 freely provided by the NASA Goddard Earth Sciences (GES) Data and Information Services Center
199 (DISC). The horizontal resolution of this dataset (level 3) is $0.25^\circ \times 0.25^\circ$ latitude-longitude and the
200 time resolution is every 3 h. In this study, [we used this satellite data to verify rainfall distribution](#)
201 [over the coastal sea due to the limitation of the observation station network, we only have the](#)
202 [observation stations inland, as shown in the figure. 1d and fig. 1e.](#) ~~This dataset was downloaded~~
203 from 1200 UTC 8 to 1200 UTC 11 December 2018 to analyze the D18 event.

Formatted: Font: 12 pt, Font color: Green

204 (b) The Himawari satellite images

205 The color-enhanced infrared imageries are designed mainly for the detection of convective
206 clouds, including those from the Himawari-8 satellite. The different colours represent different
207 cloud-top heights. Therefore, we have used these images to discern deep convection in convective
208 clouds and precipitating clouds based on their characteristics. In this study, the dataset was
209 downloaded from the Central Weather Bureau website, Taiwan, with a time resolution of 1 h.

210 2.1.5 Radar data

211 The column-maximum radar reflectivity data are one indispensable data source to identify
212 precipitation and verify model results. The reflectivity data (in dBZ) cover a wide range and the
213 values indicate rainfall intensity (the higher the dBZ, the stronger the intensity of precipitation).
214 Therefore, we used the column-maximum radar reflectivity data over central Vietnam at 1-h
215 intervals over 8-11 December 2018 to estimate the rainfall intensity during the D18 event. This
216 dataset is provided by the Mid-central Regional Hydro-Meteorological Centre of Vietnam.

217 2.1.6 The Vietnam Gridded Precipitation (VnGP) Dataset.

218 The VnGP data are derived base on the daily observed data from 481 rain gauges cross
219 Vietnam. This dataset has a resolution of 0.1° and covers the period of 1980-2010 (Nguyen-Xuan et
220 al., 2016). In this study, this dataset is used to depict the rainfall climatology in Vietnam.

221 2.1.7 The Oceanic Niño Index (ONI) data

Formatted: Font: Italic

222 The Oceanic Niño Index (ONI) data was made and provided freely by NOAA Climate
223 Prediction Center (CPC). The ONI data was computed by three month running mean of NOAA
224 ERSST.V5 SST anomalies in the Niño 3.4 region (5N-5S, 120-170W), based on changing base
225 period which onsist of multiple centered 30-year base periods. The ONI is the most commonly used
226 indices to define El Niño and La Niña events. This study used the ONI data for Niño 3.4 region to
227 define the ENSO phase of 2018. This data is available at:

228 <https://psl.noaa.gov/data/correlation/oni.data>

Formatted: Font color: Green

Formatted: Font color: Green

229 **2.2 Model description and experiment setup**

230 The Cloud Resolving Storm Simulator (CReSS, version 3.4.2), developed by Nagoya
231 University, Japan (Tsuboki and Sakakibara, 2002, 2007) is used for numerical simulation of the
232 D18 event. This model is a non-hydrostatic and compressible cloud model, designed for simulation
233 of weather events at high (cloud-resolving) resolution. In the model, the cloud microphysics is
234 treated explicitly at the user-selected degree of complexity, such as the bulk cold-rain scheme with
235 six species: vapor, cloud water, cloud ice, rain, snow, and graupel (Lin *et al.*, 1983; Cotton *et al.*,
236 1986; Murakami, 1990, 1994; Ikawa and Saito, 1991). Other subgrid-scale processes parameterized,
237 such as turbulent mixing in the planetary boundary layer, as well as physical options for surface
238 processes, including momentum/energy fluxes, shortwave and longwave radiation are summarized
239 in Table 1.

240 To study the D18 event and investigate the role played by the local terrain in this event using
241 the CReSS model, two experiments were performed using the same model domain setting, physical

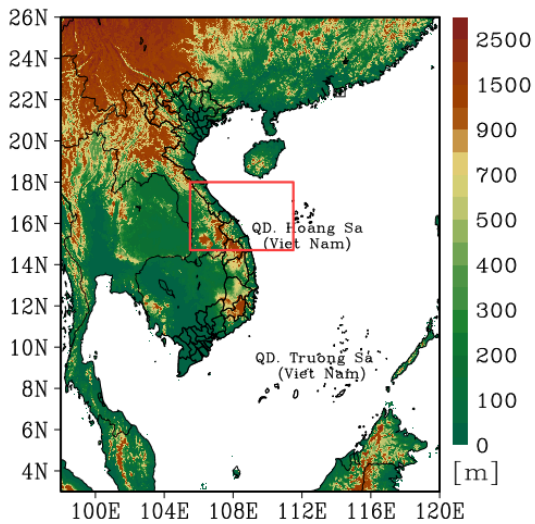
242 options, and initial and boundary conditions. Specifically, both experiments using a single domain
243 at 2.5-km horizontal grid spacing and a (x, y, z) dimension of 912 x 900 x 60 grid points (Table 1,
244 cf. Figure 2). As introduced in subsection 2.1.1, the NCEP GDAS/FNL Global Gridded Analyses
245 and Forecasts (0.25° x 0.25°, every 6 h, 26 pressure levels) was used as the IC/BCs of the model.
246 These experiments were started from 0600 UTC 8 to 0000 UTC 13 December 2018 (for a
247 simulation length of 114 h).

248 The only different setting between these experiments is at the lower boundary, the real terrain
249 data at (1/120°) resolution (roughly 0.9 km) was provided for the control simulation (CTRL) while
250 this was ignored for the sensitivity test without the terrain (NTRN).

Formatted: Font color: Green

251 The CReSS model is also designed to be run on large computers at high efficiency. Heretofore,
252 this model has been applied to study tropical cyclones, heavy rainfall events, and many other
253 convective systems (e.g., Ohigashi and Tsuboki, 2007; Yamada *et al.*, 2007; Akter and Tsuboki,
254 2010, 2012; Wang *et al.*, 2015).

255 To study the D18 event and investigate the role played by the local terrain in this event using
256 the CReSS model, two experiments were performed starting from the same initial time of 0600
257 UTC 8 December 2018. One is the control simulation (CTRL) with full terrain and the other is the
258 sensitivity test without the terrain (NTRN). The simulation domain is depicted in Fig. 3. The basic
259 main information of these two experiments, including the domain setup and model configuration, is
260 listed in Table 1.



261

262 **Figure 23:** The simulation domain of the CReSS model and topography (m) used in this study. The
 263 red box marks the study area.

264 **Table 1.** The basic information of experiments.

Domain and Basic setup	
Model domain	3°–26°N; 98°–120°E
Grid dimension (x, y, z)	912 × 900 × 60
Grid spacing (x, y, z)	2.5 km × 2.5 km × 0.5 km*
Projection	Mercator
<u>IC/BCs (including SST)</u>	<i>NCEP GDAS/FNL Global Gridded Analyses and Forecasts (0.25° × 0.25°, every 6 h, 26 pressure levels)</i>
<u>Simulation length</u>	<u>114 h</u>
Topography (for CTRL only) and sea surface temperature (SST)	Real Digital elevation model by JMA at (1/120)° and NCEP analyses (0.25° × 0.25°) spatial resolution
<u>Simulation length</u>	<u>114 h</u>
<u>Output frequency</u>	<u>1 hour</u>
Model physical setup	

Formatted: Font color: Green

Formatted: Left

Formatted: Left

Formatted: Left

Formatted: Left

Formatted: Font color: Green

Formatted: Left

Formatted: Font color: Green

Cloud microphysics	Bulk cold-rain scheme (six species)
<u>PBL parameterization</u>	<u>1.5-order closure with prediction of turbulent kinetic energy (Deardorff, 1980; Tsuboki and Sakakibara, 2007)</u>
<u>Surface processes</u>	<u>Energy and momentum fluxes, shortwave and longwave radiation (Kondo, 1976; Louis et al., 1982; Segami et al., 1989)</u>
<u>Soil model</u>	<u>41 levels, every 5 cm deep to 2 m</u>

265 * The vertical grid spacing (Δz) of CReSS is stretched (smallest at bottom) and the averaged value is

266 given in the parentheses

267 **2.3 Verification of model rainfall**

268 In order to verify the model-simulated rainfall, some verification methods are used, including

269 (1) visual comparison between the model and the observation (from the 69 automated gauges over

270 the study area), and (2) the objective verification using categorical skill scores at various rainfall

271 thresholds from the lowest at 0.05 mm up to 900 mm for three-day total. These scores are listed in

272 Table 2 along with their formulas, perfect value, and worst value, respectively. To apply these

273 scores at a given threshold, the model and observed value pairs at all verification points (gauge sites

274 here, = N) are first compared and classified to construct a 2×2 contingency table (Wilks, 2006). At

275 any given site, if the event takes place (reaching the threshold) in both model and observation, the

276 prediction is considered a hit (H). If the event occurs only in observation but not the model, it is a

277 miss (M). If the event is predicted in the model but not observed, it is a false alarm (FA). Finally, if

278 both model and observation show no event, the outcome is correct negative rejection (CNR). After

279 all the points are classified into the above four categories, the scores can be calculated by their

280 corresponding formula in Table-22 (where CN is not used).

281

282

283

284 **Table 2.** List of the categorical skill scores and their formulas.

Name of skill score	Formula	Perfect score	Worst score
Bias Score (BS)	$(H+FA)/(H+M)$	1	0 or $N - 1$
Probability of Detection (POD)	$H/(H+M)$	1	0
False Alarms Ratio (FAR)	$FA/(H+FA)$	0	1
Threat Score (TS)	$H/(H+M+FA)$	1	0

285

286 In addition to the categorical scores, the Fractions Similarity Skill Score (FSSS, Roberts and
287 Lean, 2008; Wang et al., 2022) is also applied to evaluate the model rainfall results, as**Formatted:** Font color: Green**Formatted:** Font color: Green

288
$$SFSS = 1 - \frac{\frac{1}{N} \sum_{i=1}^N (F_i - O_i)^2}{\frac{1}{N} \sum_{i=1}^N F_i^2 + \frac{1}{N} \sum_{i=1}^N O_i^2} \quad (1)$$
289

290 where N is the total number of verification points, F_i is the forecast value, and O_i is the observed
291 value, at the i th point among N, respectively. SSS is used to measured against the worst the mean
292 squared error (MSE) possible. The formula shows that a forecast with perfect skill has a FSS of 1,
293 while a score of 0 means zero skill.**Formatted:** Font color: Green**Formatted:** Font color: Green294

3 Overview of the D18 Event

295

3.1 Rainfall and its distribution

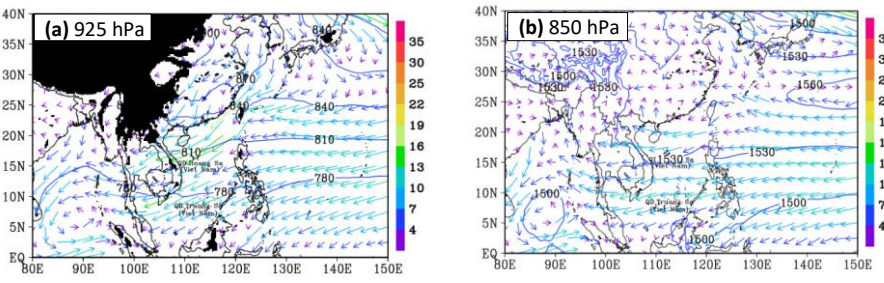
296 As introduced earlier, during 8–12 December 2018, an extreme precipitation event occurred in
297 central Vietnam. The maximum accumulated rainfall was recorded from 9 to 11 December with a
298 peak daily rainfall greater than 500 mm and 72-h accumulated rainfall exceeds 800 mm (Figs. 1a-d).
299
300 Besides, the daily and 72-h rainfalls observed at 69 stations show that the extreme precipitation
301 occurred along the eastern coastal plains, on the windward-eastern side of the Truong Son Range.
302 Especially over Quang Nam province, where the Truong Son Range reaches its highest of over 2500
303 m (Figs. 1a-d). In addition, satellite products from the Tropical Rainfall Measuring Mission (TRMM)**Formatted:** Font color: Green

304 seriously underestimates the D18 event (Fig. 1e), but indicates that the rainfall occurred not only in
305 coastal plains but also over the nearby ocean.

306 3.2 Synoptic conditions

307 ~~In this subsection, the synoptic scale atmospheric conditions during the D18 event are~~
308 ~~analyzed.~~ During the D18 event, the horizontal winds at 925 hPa (averaged from 0000 UTC 8 to
309 1800 UTC 11 December) over central Vietnam and the SCS are characterized by a strong
310 convergent zone between the northeasterly winds blowing from northeastern China into northern
311 SCS and central Vietnam, and the easterly winds blowing from the western North Pacific (WNP)
312 into the SCS (Fig. 34a). The wind speed over northern SCS and central Vietnam is over 13 m s^{-1} .
313 At 850 hPa, horizontal winds are predominantly easterly, with speeds of about $10\text{--}13 \text{ m s}^{-1}$ (Fig.
314 34b). At 500 hPa, central Vietnam is affected by southeasterly winds that originated from the
315 easterly winds over the WNP (Fig. 34c). ~~Besides, Figure 3 also indicates that there was no existence~~
316 ~~of any tropical cyclone during the D18 event. Therefore, tropical cyclones or the combined effect of~~
317 ~~cold surges originating from northern China and tropical depressions that have been mentioned as~~
318 ~~one of the patterns that cause heavy rainfall in central Vietnam is not the mechanism of the D18~~
319 ~~event.~~

Formatted: Font color: Green



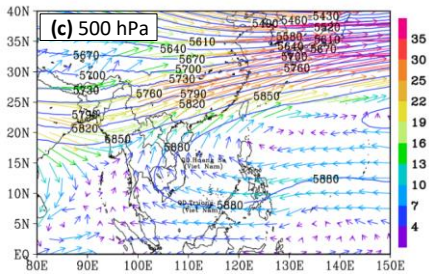
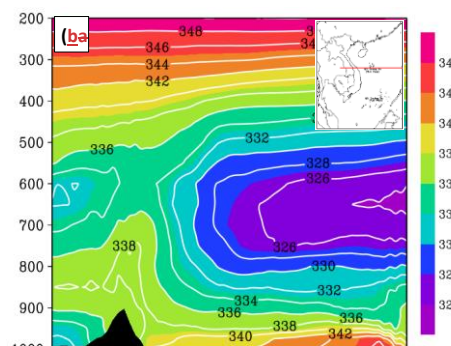
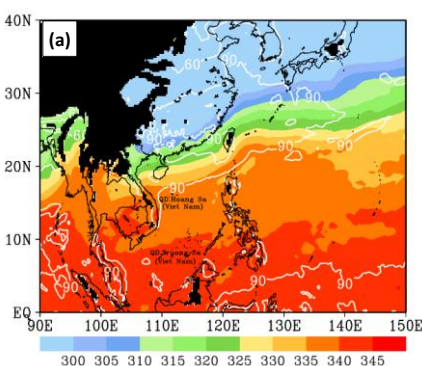


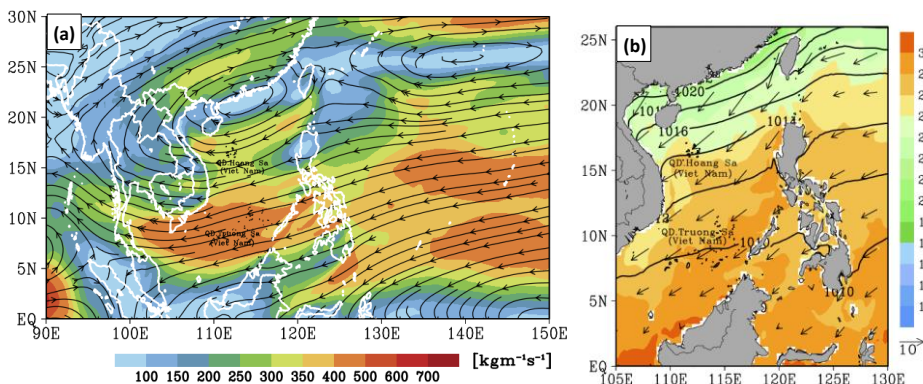
Figure 34. (a) The ERA5 averaged horizontal wind vectors (m s^{-1} , color for speed) and geopotential height (gpm, blue contours, every 30 gpm) at the 925 hPa from 0000 UTC 8 to 1800 UTC 11 December 2018. (b) As in (a), but for the 850 hPa. (c) As in (a), but for the 500 hPa. The blacked areas are where the 925-hPa level is below the ground.

From a thermodynamic perspective, the equivalent potential temperature (θ_e) field at 925 hPa shows that a warm and moist tropical air mass exist in central and SCS with θ_e values greater than 335 K, and the relative humidity is around 90 % during the D18 event (Fig. 45a). The high moisture content combines with a decrease in θ_e with altitude, indicating convective instability in the lower atmosphere below about 500 hPa (Fig. 45b). Furthermore, the interaction between northeasterly and easterly winds seemed to enhance instability in the lower atmosphere.



331 **Figure 45.** (a) The ERA5 averaged equivalent potential temperature (K, color), and relative
 332 humidity (%, white contours, every 30 %) at 925 hPa. The blacked areas are where the 925-hPa
 333 level is below the ground. (b) the east-west vertical cross-section along 16°N (see insert) of
 334 averaged equivalent potential temperature (θ_e , K, color, every 5 K), from 0000 UTC 8 to 1800 UTC
 335 11 Dec 2018. The topography is dark shaded.

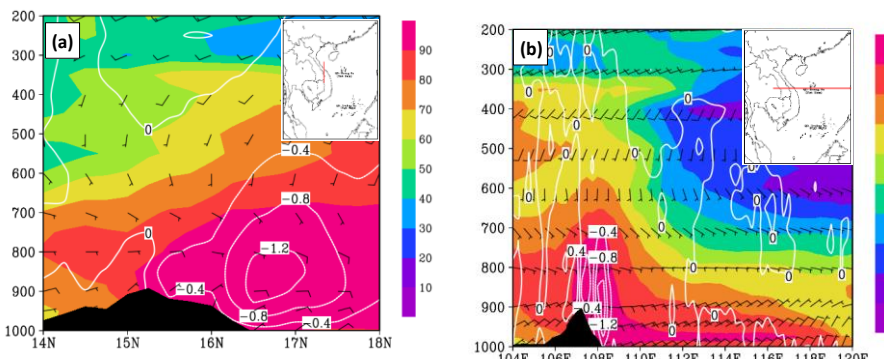
336 The above analysis suggests that the northeasterly, easterly, and southeasterly winds (cf. Figs.
 337 34a-c) all played an important role in transported unstable air into central Vietnam. Particularly,
 338 when the strong northeasterly and the easterly winds at low levels and southeasterly wind at upper
 339 levels blow into central Vietnam, they bring warm, moist, and unstable air into central Vietnam.
 340 This moisture is transported to central Vietnam by strong moisture flux through the deep column
 341 from the WNP, across the Philippines and the SCS (Fig. 56a). Furthermore, the high SST of the
 342 SCS (>27° C) also help to enhance and maintain abundant moisture during this event (Fig. 56b).



343
 344 **Figure 56.** (a) The ERA5 averaged surface–200-hPa vertically integrated moisture flux ($\text{kg m}^{-1} \text{s}^{-1}$).
 345 (b) the ERA5 averaged SST ($^{\circ}\text{C}$, color), mean sea-level pressure (hPa, isobars, every 2 hPa), and
 346 horizontal wind vectors at 10-m height (m s^{-1} , vector), from 0000 UTC 8 to 1800 UTC 11 Dec
 347 2018.

348 Consequently, the atmospheric conditions and local topographic characteristics in interaction
 349 result in moisture convergence and forced uplift in the lower troposphere during the D18 event.
 350 This can be seen in Fig. 67, where extensive rising motion occurs in the lower troposphere along
 351 coastal Vietnam, with a maximum value of -1.2 Pa s^{-1} . Besides, Figs. 67a,b also indicate that the
 352 strong northeasterly wind along with warm, moist and unstable air is blocked by the Truong Son
 353 Range. This pattern suggests that the Truong Son Range also played an important role in the
 354 development of heavy rainfall in central Vietnam in D18. In detail, when the northeasterly and
 355 easterly winds at low levels blow into central Vietnam and become block by the Truong Son Range,
 356 which is located along the border of Vietnam and Laos, forced uplift is resulted at the windward
 357 side, with downward motion over the lee side (in Laos, Fig. 67b). Furthermore, the low-level
 358 convergence in this event was strong enough (Fig. 3a), and the air was unstable enough (Fig. 4b) to
 359 trigger most of the convection near the shoreline (further inland, Fig. 6a)

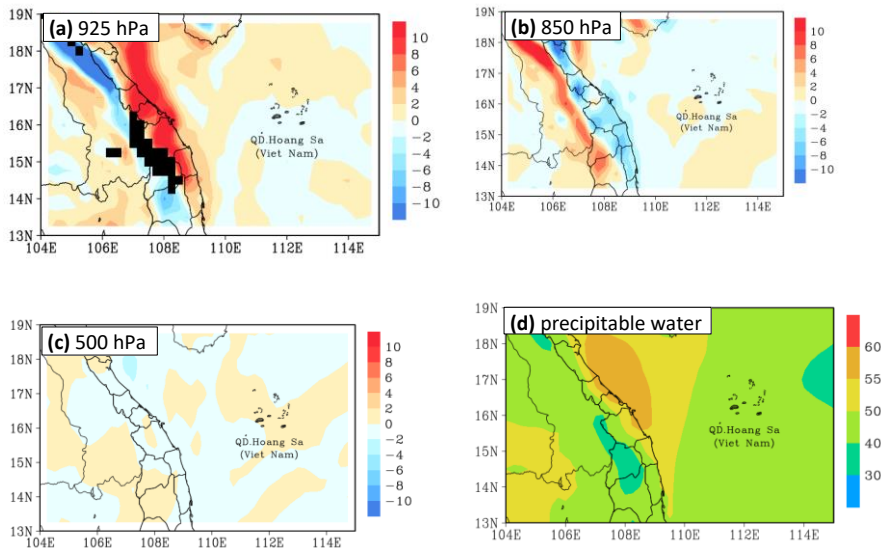
360



361 **Figure 67.** (a) The ERA5 the south-north vertical cross-section along 107.5°E (see insert) of
 362 averaged horizontal wind (m s^{-1} , vectors) and vertical motions (Pa s^{-1} ; white contours, negative for
 363 upward motion), and relative humidity (%), shaded), from 0000 UTC 8 to 1800 UTC 11 Dec 2018.
 364 The topography is dark shaded. (b) As in (a), but for the vertical cross-section along 16°N .

365 As described above, when the strong northeasterly and easterly winds at low levels blow into
 366 central Vietnam, they bring warm, moist, and unstable air that originated in the WNP and is
 367 enhanced over the SCS. Then, this air is blocked by the Truong Son Range, which has a height of
 368 around 2 km, leading to forced convergence and upward motion at low levels and divergence
 369 further above. These conditions consequently lead to moisture flux convergence of over 8×10^{-4} g
 370 $\text{kg}^{-1} \text{s}^{-1}$ at 925 hPa (Fig. 78a) and moisture flux divergence at 850 hPa with comparable magnitudes
 371 (Fig. 78b). This divergence reduces sharply further up toward the middle and upper levels (Fig.
 372 78c). These factors create a moist atmosphere with a precipitable water amount (through the deep
 373 column) exceeding 50 mm during the D18 event (Fig. 78d). The above atmospheric ingredients and
 374 characteristics in local topography in combination created favorable environmental conditions to
 375 trigger orographic rainfall. As a consequence, the D18 event happened.

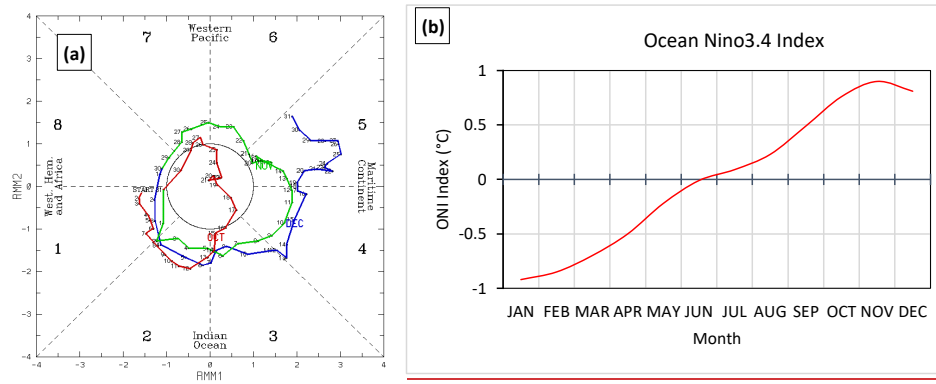
376



377 **Figure 78.** (a) The ERA5 averaged moisture convergence/ divergence ($\times 10^{-4}$, $\text{g kg}^{-1} \text{s}^{-1}$, shaded,
 378 positive for convergence) at the 925 hPa, from 0000 UTC 8 to 1800 UTC 11 Dec 2018. The blacked

379 areas are where the 925-hPa level is below the ground. (b) As in (a), but for the 850 hPa. (c) As in
380 (a), but for the 500 hPa. (d) The ERA5 averaged precipitable water between surface and 200 hPa
381 (mm), from 0000 UTC 8 to 1800 UTC 11 Dec 2018.

382 Besides investigating the synoptic-scale atmospheric conditions above, this study also verified ← Formatted: Indent: First line: 0.31"
383 the impact of intraseasonal oscillations in the tropical atmosphere on the D18 event. To be more
384 specific, figure 8a reveals that the MJO in Western Pacific was not active in early December 2018
385 as well as during the D18 event. Figure 8b indicates that the last three months of 2018 are a fairly
386 weak El Niño phase. In addition, previous studies showed that central Vietnam had less rainfall in
387 the El Niño years. Therefore, MJO and ENSO are also not the cause and have no impact on the D18
388 event.



389 Figure 8. (a) The Madden-Julian Oscillation (MJO) location and the strength through 8 different
390 areas along the equator around the globe. Labelled dots for each day. Red line is for October, Green
391 line is for November, Blue line is for December. Source: Commonwealth of Australia 2019, Bureau
392 of Meteorology. (b) The Oceanic Niño Index (ONI) of the Niño 3.4 region (5°N-5°S, 120°W-170°
393 W) for 2018.

394 3.3 Evolution of precipitating clouds The local thermodynamic conditions prior the D18 event

Formatted: Font color: Green

Formatted: Font color: Green

395 In this part, the local thermodynamic conditions that led to the D18 event are analyzed. Figure 98
396 shows these conditions at 1200 UTC 8 December 2018. At this time, it is quite warm and moist
397 over central Vietnam and the SCS, with θ_e of at least 335 K (Fig. 9a). As mentioned, this moisture
398 is transported to central Vietnam from the WNP by the strong moisture flux, across the Philippines
399 and the SCS and eventually intercepted by the Truong Son Range at the western border of Vietnam
400 (Figs. 9b,e). The thermodynamic conditions and local orography in interaction lead to a moist
401 atmosphere with a precipitable water amount exceeding 50 mm (Fig. 9d). Furthermore, the vertical
402 wind profile also indicates both warm advection at low levels (veering winds with height) and a
403 considerable southerly wind shear between 950 and 500 hPa (Fig. 9c). These thermodynamic
404 conditions were favorable for the development of convection and precipitation, there is a strong
405 convergence zone of the low-level northeasterly wind carrying the moisture over the north of the
406 study area and near the shoreline (Figs. 9a,b). The northeasterly wind convergence led to a low-
407 level moisture convergence both inland and over the coastal sea. This happened as the low-level
408 northeasterly wind carrying the moisture blew to central Vietnam and interacted with local
409 topography, the low-level northeasterly flow reduced in speed over a wide area (refers to figs. 6),
410 leading to a strong moisture flux convergence at low-level both inland and near the shoreline and
411 moisture flux divergence at the upper level (figs. 9c, d). Due to the convergence of northeasterly
412 wind and moisture happened mainly in the north of latitude 16, the rising motion in the south of
413 latitude 16 mainly happened at low-level (less than 700 hPa, fig. 9e) due to blocked by the Truong
414 Son range. Furthermore, this process occurred in a warm and unstable atmosphere (refer to figs. 4),
415 making a favourable environmental condition to trigger most of the convection near the shoreline
416 instead of over the slopes (further inland) by forced uplift of the terrain. Hence, precipitable water
417 between the surface and 200 hPa exceeding 55 mm just formed over the coastal zone of the north of
418 the study area (fig. 9f). Consequently, heavy rainfall only concentrated around the coastal zone.
419 These analyses are suitable for satellite and radar data.

Formatted: Indent: First line: 0", Space Before: 0 pt,
After: 8 pt

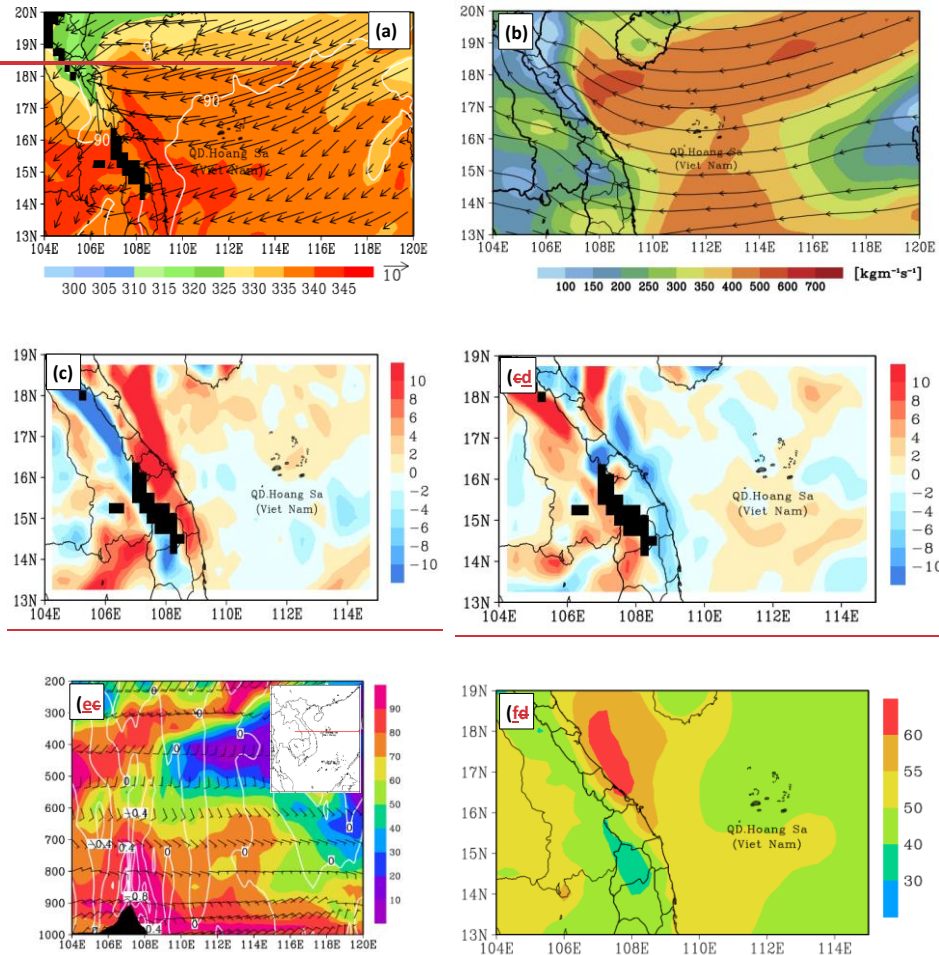
Formatted: Font: 12 pt

Formatted: Font: (Default) Times New Roman

Formatted: Font: (Default) Times New Roman

Formatted: Font: (Default) Times New Roman

420 **Formatted Table**



421 **Figure 9.** (a) The ERA5 θ_e (K, shaded), horizontal winds (m s^{-1} , vector), and relative humidity (%,
422 white contours, every 30 gpm) at 925 hPa. The blacked areas are where the 925-hPa level is below
423 the ground. (b) Surface-200-hPa vertically integrated moisture flux ($\text{kg m}^{-1} \text{s}^{-1}$). (c) East-west vertical cross-
424 section along 16°N (see insert) of vertical motions (Pa s^{-1} , white contours), relative humidity (%,

425 shaded), and horizontal winds (m s^{-1} , vector). The topography is black shaded. (d) Precipitable
426 water between surface and 200 hPa (mm). All panels are for 1200 UTC 8 Dec 2018.

427 To be more specific, On satellite imageries from 1200 UTC 8 to 1100 UTC 9 December (Fig.
428 S1), a series of deep convective clouds (cumulonimbi, or Cb) first form over northern and central
429 Vietnam and Laos on 8 December, with mainly a northeast-southwest to east-west alignment. With
430 blackbody temperatures (T_B) below -42°C , several isolated deep cells also develop near the coast
431 over the southern part of the study area after 0200 UTC on 9 December (Fig. S1). Generally, these
432 deep Cb clouds tend to move slowly offshore and weaken after a few hours. Meanwhile, the study
433 area is also covered by precipitating clouds known as nimbostratus (Ns) that are not as deep, with
434 cloud-top T_B at $-20^\circ\text{--}0^\circ \text{C}$ and above (Fig. S1). These Ns clouds first form over the northern part of
435 the study area and then grow and expand southward along the coast, eventually cover the entire
436 study area on 9 December (Fig. S1). As analyzed above, both deep Cb clouds and the persistent Ns
437 clouds produced long-lasting rainfall for hours, starting along the coast from 1200 to 1700 UTC 8
438 December. After that, the rain area extends both inland and over the coastal sea (Fig. S2). The
439 rainfall intensity is the greatest from 2000 UTC 8 to 0200 UTC 9 December, with a column-
440 maximum radar reflectivity (C_{\max}) $\approx 40 \text{ dBZ}$ (Fig. S2). Afterwards, the rainfall intensity decreases
441 to some extent but remain at 15-35 dBZ rather steadily (Fig. S2). While the precipitation is not too
442 intense, it falls persistently over many hours, leading to high 24-h rainfall accumulation at some
443 locations. Thus, the local thermodynamic conditions seem to maintain for many hours and lead to
444 the continuous development of precipitating clouds during much of 8 December.

445 At 1200 UTC 9 December, a warm, and moist, and unstable atmospheric is still maintained
446 over central Vietnam and the SCS, with $\theta_e > 335 \text{ K}$ (Fig. 10a and Figs. 4). The moisture continued
447 to be transported from the east, with the northeasterly wind played the main role in this transport
448 (Fig. 10b). These moisture conditions are associated with the northeasterly wind over central
449 Vietnam seemed stronger than the previous day, leading to a stronger low-level uplifting than that

Formatted: Font color: Green

450 on 8 December (Fig. 10c). Consequently, the atmosphere becomes moister with increases
451 precipitable water amount to over 55 mm (Fig. 10d). However, the strong convergence of the low-
452 level northeasterly wind carrying the moisture in Ha Tinh and Quang Tri provinces moved
453 southward to Quang Tri and Quang Nam provinces (Fig. 10a). This moving dragging along the
454 move of the low-level moisture convergence (Figs. 10c,d). Besides, Fig. 9e shows that the low-level
455 uplifting motion is stronger than the previous day due to most of the strong northeasterly wind zone
456 blocked by the Truong Son range. Besides, the southward movement of the northeasterly wind and
457 moisture convergence zone also led to the southward movement of precipitable water between the
458 surface and 200 hPa to the coastal zone between Quang Binh and Quang Tri provinces (Fig. 10f).
459 As a result, the main heavy rainfall also moved southward to this area. This also coincides with
460 observed satellite and radar data. Moreover, These thermodynamic conditions played a role to
461 sustain the development of precipitating clouds on 9 December. In detail, On this day (since 1200
462 UTC), satellite imageries also show some characteristics of deep convection over the coastal area
463 (Fig. S3), but the cloud top temperatures, in general, are not as cold as on 8 December. Meanwhile,
464 the lower precipitating Ns clouds cover much of the study area from 1200 UTC 9 to 0300 UTC 10
465 December, then gradually disintegrate (Fig. S3). These clouds kept producing rainfall for the whole
466 day, with the higher C_{max} values (~40 dBZ) and rainfall intensity from 1200 UTC 9 to around 0000
467 UTC 10 December (Fig. S4), mainly over the coastal plain and nearby sea. After that, the rain
468 gradually decreases in both intensity and areal coverage.

469

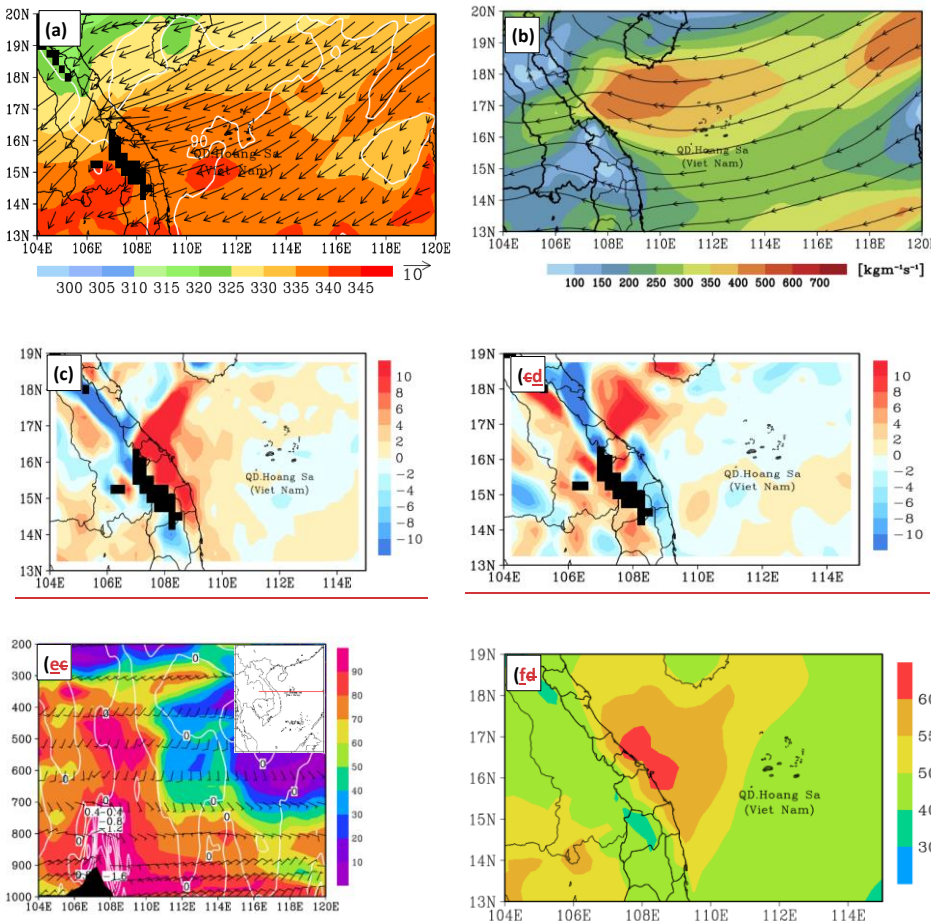
470

471

472

473

← Formatted: Indent: First line: 0"



Formatted Table

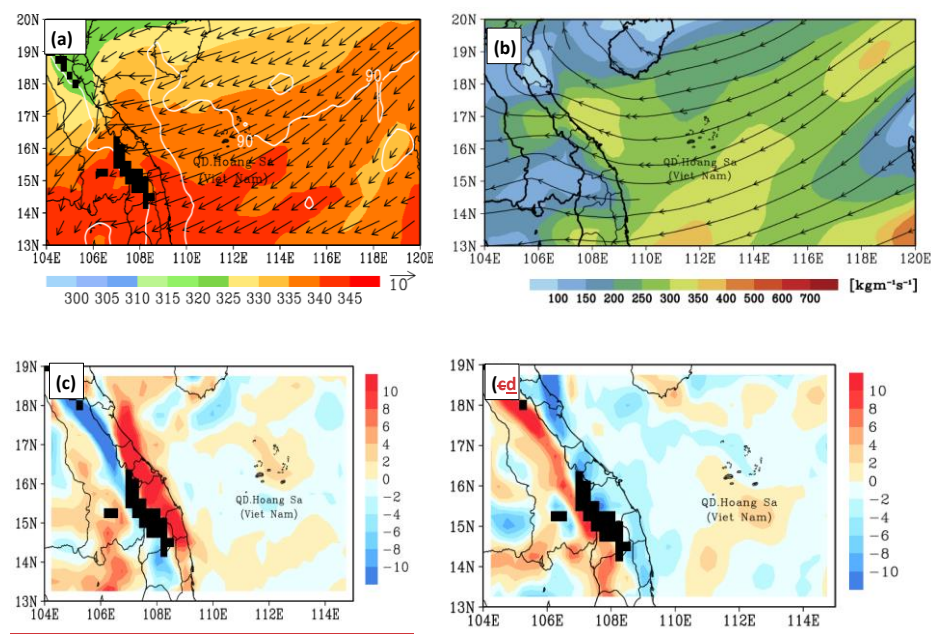
474 **Figure 10.** As in Fig. 9, except for 1200 UTC 9 Dec 2018.

475 At 1200 UTC 10 December, the atmosphere remains very moist with a precipitable water
 476 amount of 55 mm (Fig. 11d). Some of the local dynamical and thermodynamically parameters,
 477 however, are reduced from one day earlier and become not as favorable, including the velocity of
 478 northeasterly wind, the upward motion over central Vietnam (Fig. 11c), and moisture flux (Fig.
 479 11b), and precipitable water amount (Fig. 11f). Hence, the development of precipitating clouds also
 480 reduces significantly on this day and mostly exist offshore over the ocean (Fig. S5). Compared to

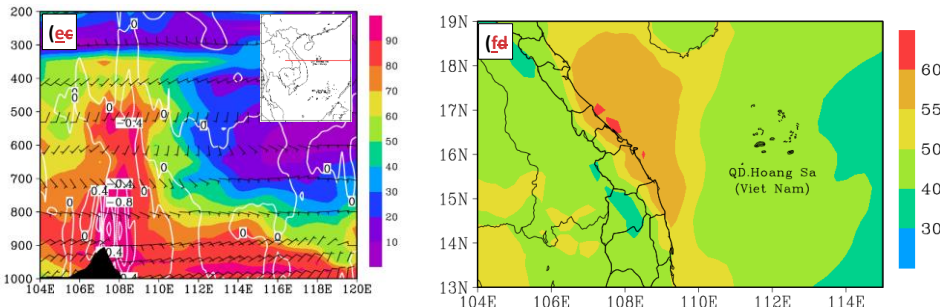
Formatted: Font: (Default) Times New Roman, 12 pt,
 Font color: Green

Formatted: Font color: Green

481 the past two days, the development of convective cells is also reduced. Near the coast, only three
 482 convective cells developed on 10 December, one at 1400 UTC, the second at 2000 UTC, and the
 483 third one shortly after 2200 UTC. Also, moving eastward and offshore after formation, these
 484 relatively small cells spend only 1-3 h over land. In general, the environmental conditions become
 485 less favorable for developing rain clouds after 1200 UTC 10 December. Consequently, there is a
 486 significant decrease in rainfall, which occurs mainly during 1200-1600 UTC then weaken with time
 487 (Fig. S6).



Formatted Table



488 **Figure 11.** As in Fig. 9, except for 1200 UTC 10 Dec 2018.

489

490 **4 Model Simulation Results**

491 In this section, the model simulation results are used to investigate the role of topography in
 492 the development of clouds and rainfall in the D18 event, and the CReSS model is also evaluated for
 493 its ability to reproduce the event over the study area.

494 Figure 12 presents the daily averaged surface horizontal winds and daily rainfall in CTRL and
 495 NTRN for each of the three days from 9 to 11 December 2018. In CTRL, the model has well
 496 simulated the surface wind. As a result, the model produced a maximum 24-h rainfall of around
 497 400 mm on 9 December (Fig. 12a), roughly comparable in magnitude to the observation (Fig. 12c).

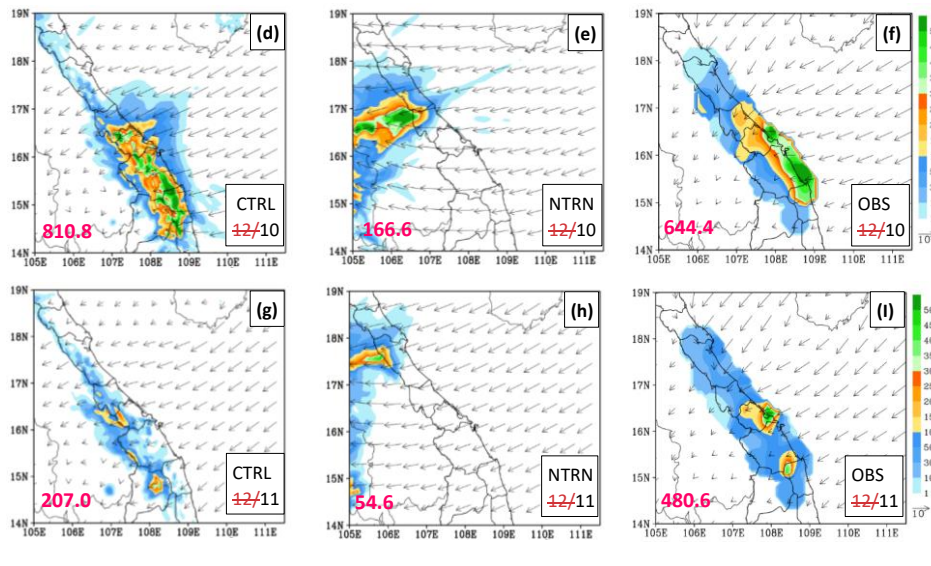
498 While one should bear in mind that the limited number of rain gauges have a smaller coverage area
 499 and cannot resolve the detailed distribution of rainfall (cf. Fig. 1a2b), the model rainfall in CTRL is
 500 slightly more offshore north of 16° N but more inland near 16° N, thus is not as abundant along the
 501 coast compared to the observation. In other words, model rainfall has some location errors but the
 502 magnitude is comparable by visual inspection. For surface winds, their direction and magnitude are
 503 well simulated by the CTRL experiment (Fig. 12).

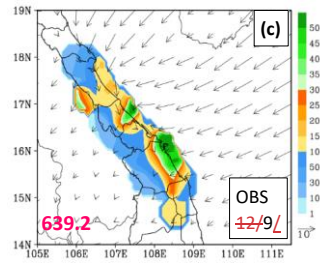
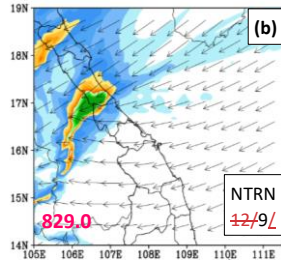
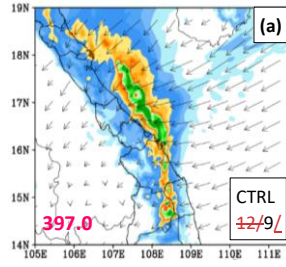
504 An objective and more quantitative verification of model rainfall can be provided by the threat
 505 score (TS) computed at the rain-gauge sites, which shows that the model has high score at low

506 thresholds of ≤ 10 mm (per 24 h) but gradually decreases toward higher thresholds (Fig. 13a, red
 507 curve). In particular, the TS is about 0.5 at 25-50 mm, below 0.2 above 160 mm, and about 0.1 at
 508 350 mm. Eventually, the TS drops to zero at 500 mm, which is not too far from the observed peak
 509 rainfall of over 500 mm (at Da Nang, cf. Fig. 1a). The bias score (BS) confirms that the model does
 510 not produce enough rainfall over the coastal plains, as its value drops from about 1.0 at 0.05 mm to
 511 below 0.4 at and above 250 mm. As another objective measure of overall quality of prediction, the
 512 **fraction-Similarity-skill score (FSSS)** is about 0.5 for 9 December. Overall, the model appears to
 513 produce too much rainfall offshore north of 16° N and not enough rainfall along the coast, and this
 514 might be to some extent linked to its surface wind coming more from the east-northeast, compared
 515 to northeast in the ERA5 analysis (Figs. 12a,c), leading to somewhat different locations of low-level
 516 convergence of wind and moisture.

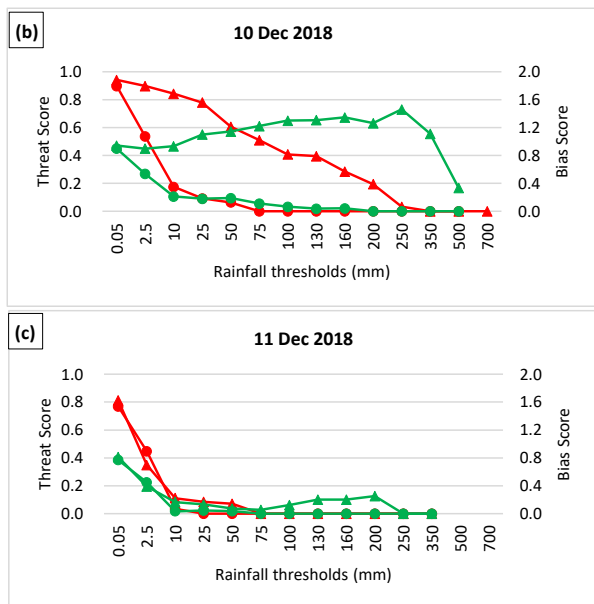
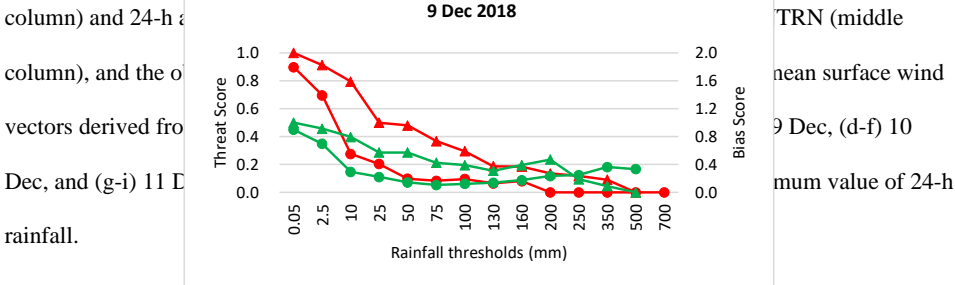
Formatted: Font: (Default) Times New Roman, 12 pt,
 Font color: Green

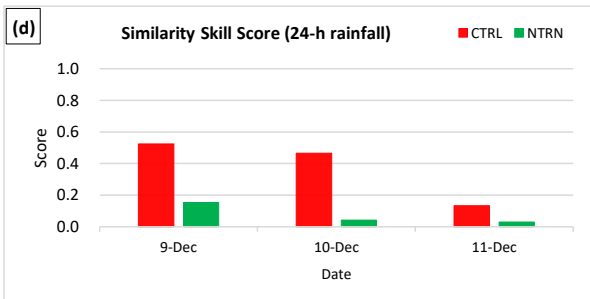
Formatted: Font color: Green





517 **Figure 12.** Simulated daily-mean surface horizontal wind vectors (m s^{-1} , reference length at right





523 **Figure 13.** (a)-(c) The threat scores (red) and bias scores (green) of 24-h accumulated rainfall for
 524 the CTRL (curve with triangles) and NTRN (curve with dots) experiments for the three days of 9-11
 525 Dec 2018. (d) Fractions skill scores of 24-h accumulated rainfall for the two experiments.

Formatted: Font color: Auto

526 For 10 December, while similar differences in prevailing surface winds still exist between
 527 model simulation and ERA5 data, the model captured the southward movement of the northeasterly
 528 wind. Therefore, the model had well captured the southward movement of the main heavy
 529 rainfallthe model. The rainfall location has improved with better agreement with the observation
 530 (Figs. 12d,f), but in general slightly more inland and not right on the coast. Both over 600 mm, the
 531 observed and simulated peak daily rainfall values are again comparable. Due to the improvement in
 532 spatial pattern, the TSs exhibit higher values than those for the previous day across low to middle
 533 thresholds (up to 200 mm) but reduce to zero at 250 mm (Fig. 13b), while the FSSS (near 0.46) is
 534 only slightly reduced (Fig. 13d). In agreement with the better TS values, the BS remains between
 535 0.8 and about 1.4 from low thresholds up to 350 mm, and drops to about 0.35 at 500 mm (Fig. 13b).

Formatted: Font color: Green

536 For 11 December, the model does not simulate well the rainfall field, as its rainfall is displaced
 537 toward the Truong Son Range (and the border to Laos), instead of over the coastal plain as observed
 538 (Figs. 12g,i). The spatial coverage of model rainfall is smaller and the peak amount (~200 mm) also
 539 lower compared to the rain-gauge data, while the surface wind appears weaker than the ERA5 data
 540 as well. While the observed peak amount became lower as the D18 event was coming to an end, the

541 TSs also decrease rapid with threshold, and are close to 0.1 at just 10 mm and become zero at and
542 above 70 mm (Fig. 13c). Consistent with the inadequate amount over land, the BSs also decrease
543 rapidly with thresholds, from about 0.8 at 0.05 mm to below 0.3 over 100-200 mm. For this day, the
544 **FSSS** is only about 0.14 and significantly lower than the values for 9 and 10 December (Fig. 13d).

Formatted: Font color: Green

545 Likely also related to the weaker surface winds in the model, the less-than-ideal results of rainfall
546 may be also affected by the longer range of integration, at 66-90 h, for 11 December.

547 To test the impact of topography in the D18 event, the NTRN experiment was carried out.

548 Without the terrain, **the model had not good simulated the surface wind. Consequences**, the rainfall
549 as simulated by CReSS would be displaced much more inland from the coastal region for all three
550 days of 9-11 December (Figs. 12b,e,h), and more importantly, the pattern would no longer be
551 elongated and parallel to the coast, even though the peak amounts are similar to the observation.
552 Thus, the topography was fundamental in determining the basic rainfall area and pattern in the D18
553 event. With incorrect distributions, the TS values (Fig. 13, green curves) are much lower and drop
554 to below 0.2 at thresholds above 10-25 mm for all three days. The thresholds at which the TSs
555 decrease to zero are 200, 75, and 25, respectively for the three days, and much lower than those in
556 the CTRL, especially for 9 and 10 December. The BS values in the NTRN also tend to be lower
557 than those in the CTRL, sometimes much lower, reflecting its incorrect location and thus little
558 rainfall at gauge sites with rainfall in reality. The **FSSS** values are also much lower, with values
559 near 0.16, 0.04, and 0.04 for the three days. Without the topography, the surface wind pattern near
560 the coast and over land would be much stronger and very different, due to the lack of its blocking
561 and uplifting effects, and also the associated thermodynamic effects.

Formatted: Font color: Green

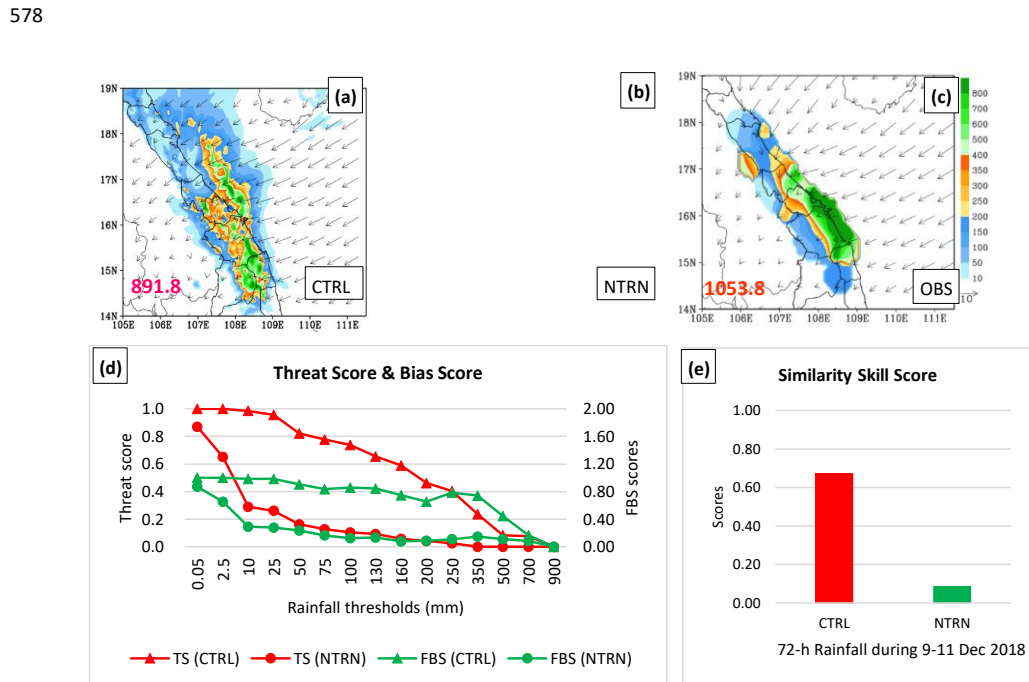
562 For the D18 event as a whole, the three-day total rainfall distribution produced by the model
563 compares quite favorably with the observation in both quantity and spatial pattern (Figs. 14a,c),
564 with generally minor displacement errors more toward inland **at around 15°-16° N. Despite these**
565 **errors, the spatial distribution of rainfall in the model corresponds well to the zone of low-level**

Formatted: Font color: Green

Formatted: Font color: Green

566 moisture convergence in the ERA5 analysis (Fig. 78a). In agreement with visual assessment, the
 567 TSs of the 72-h QPFs are quite high across even heavy-rainfall thresholds: around 0.8 at 100 mm
 568 (per 72 h), close to 0.5 at 200 mm, above 0.2 at 350 mm, and 0.1 at 700 mm, with an overall SFSS
 569 ≈ 0.7 (Figs. 14d,e). As shown, the rainfall fields for individual days in D18 are very different
 570 without the topography in NTRN, and the same is true for the whole event (Fig. 14b). The TSs also
 571 indicate a much lower skill in QPF, with TS below 0.2 at ≥ 50 mm (per 72 h) and TS = 0 at ≥ 350
 572 mm, BS below 0.35 at ≥ 10 mm, and also an overall SFSS of less than 0.1 (Figs. 14d,e). The results
 573 in Figs. 12 and 14 also indicate a significant wind-blocking effect by the Truong Son Range. In
 574 CTRL, the surface northeasterly winds commonly exceed 10 m s^{-1} in speed over the SCS, but are
 575 reduced significantly (and even to near-zero speed) near the Annamite Range (and in Laos). On the
 576 contrary, there is no reduction in speed as the winds blow across central Vietnam in NTRN, without
 577 the blocking effect of the topography.

578 Formatted: Font color: Green



579 **Figure 14.** (a)-(c) As in Figs. 11a-c, except for three-day averaged surface horizontal wind vectors
580 and 72-h accumulated rainfall over 9-11 Dec 2018. (d), (e) As in Figs. 12c,d, except for TSs and
581 FSSs of the 72-h accumulated rainfall over 9-11 Dec 2018.

Formatted: Font color: Auto

Formatted: Font color: Auto

582 5 Conclusion

583 **879.6** In this study, the extreme precipitation event that occurred on 8-12 December 2018 along the
584 coast of central Vietnam is analyzed, and the simulation results by a CRM (the CReSS model) is
585 evaluated. The major findings are summarized below.

586 Analysis on the D18 event has revealed several key factors which led to this record-breaking
587 rainfall event: First, for all four days from 8 to 11 December, the strong northeasterly winds in the
588 lower troposphere blew from the Yellow Sea into the SCS, and interacted with strong low-level
589 easterly winds (below 700 hPa) over the SCS. This interaction strengthened the upstream easterly to
590 northeasterly winds and generated strong low-level convergence, as the winds blew into central
591 Vietnam and wasere blocked by the Truong Son Range. the low-level northeasterly flow reduced in
592 speed and led to moisture flux convergence and rising motion along the coast of Vietnam
593 persistently, resulting in forced uplift near the surface over the coastal plains. Furthermore, the
594 Consequently, heavy rainfall was produced along the coast of central Vietnam. Second, the strong
595 easterly winds played an important role in transporting moisture from the WNP, across the
596 Philippines and the SCS, into central Vietnam. Third, the Truong Son Range also played an
597 important role in this event due to its barrier effect. Finally, the high SST of the SCS ($>27^{\circ}\text{C}$) also
598 acted to help replenishing the moisture in this event. This above mechanism in the D18 event is
599 different from those documented in previous studies. Particularly, according to previous studies, the
600 heavy and extreme rainfall events are usually due to the multi-interaction between the northeasterly
601 wind and preexisting tropical disturbance over the SCS and local topography or tropical cyclone or
602 impacts by ENSO or MJO. However, these factors have not appeared during the D18 event.
603 Therefore, we suggest that the interaction of the northeasterly and easterly winds in the moist,

Formatted: Font color: Green

Formatted: Font color: Green

604 unstable atmospheric and local topography can also lead to heavy precipitation events along the
605 central coastal plains of Vietnam. Another interesting finding of this study is that even though short
606 periods of heavy rainfall from deep convection also contributed, the extreme rainfall of the D18
607 event was mainly from the persistent rain from nimbostratus clouds (Ns) that do not possess a high
608 reflectivity or a very cold cloud top.

609 One of the features of the D18 event is that the main heavy rain band moved from the north to ← **Formatted:** Indent: First line: 0.31"
610 south of the study area during the event. The analysis of the local thermodynamic reveals the
611 movement of the convergence northeasterly wind zone in the north of the study area from north to
612 south. This movement dragged along the movement of the convergent moisture zone. The
613 movement of convergent moisture zone results in precipitation water column moving from north to
614 south. Consequently, the main heavy rain band moved from north to south.

615 The evaluation of model simulation results at a grid size of 2.5 km indicates the following. In the → **Formatted:** Justified, Indent: First line: 0.31", Space
616 CTRL, the model has well simulated the surface wind as well as captured the wind convergence's → **Formatted:** Font color: Green
617 southward movement. Therefore, the CReSS model has reproduced this event's rainfall field quite → **Formatted:** Font color: Green
618 well, for both daily and three-day accumulations, but with some displacement errors. In terms of
619 objective verification skill scores, in particular, CReSS displays high skills at heavy-rainfall
620 thresholds for both daily rainfall ($TS \geq 0.1$ at 200-350 mm and $FSS \approx 0.5$ for 9 and 10 December)
621 and 72-h total ($TS \approx 0.1$ at 700 mm and $FSS \approx 0.7$). However, the rainfall simulation is less ideal for
622 11 December (TS drops to zero at thresholds ≥ 75 mm), which had less rainfall and is at a longer
623 range (than the previous two days). Besides, the model also captured the southward movement of the → **Formatted:** Font color: Green
624 main heavy rain band during the event, as seen in the observed data. In the sensitivity test of NTRN → **Formatted:** Font color: Green
625 where the topography is removed, the model has poorly simulated the surface wind and did not
626 capture the southward movement of the wind convergence zone. This led to → **Formatted:** Font color: Green
627 the model produced a different rainfall pattern not along the coast as observed (and in CTRL), thus confirming the important
628 role by the Truong Son Range in this event. In addition, the evaluation of simulation results also → **Formatted:** Font color: Auto

629 shows that the CReSS model has well simulated the surface winds, both in their direction and
630 magnitude.⁷

631 Generally, these results enhanced our knowledge about the mechanisms which cause the heavy
632 rainfall in central Vietnam, as well as explained features of the D18 event. The above result also
633 shows the promising capacity of the CReSS model for research and forecast of heavy rainfall in
634 Vietnam. In a follow-up paper, a set of high-resolution time-lagged ensemble prediction is performed
635 using the CReSS model, and the predictability of the D18 event will be evaluated.

Formatted: Font color: Green

636 **Code and data availability**

637 The CReSS model used in this study and its user's guide are available at the model website at
638 http://www.rain.hyarc.nagoyau.ac.jp/~tsuboki/cress_html/index_cress_eng.html.

Formatted: Font color: Auto

Formatted: Font color: Auto

639 **Author contribution**

640 Duc Van Nguyen prepared datasets, executed the model experiments, performed analysis, and
641 prepared the first draft of the manuscript. Chung-Chieh Wang provided the funding, guidance and
642 suggestions during the study, and participated in the revision of the manuscript.

Formatted: Font color: Auto

Formatted: Font color: Auto

Formatted: Font color: Auto

643 **Competing interests**

644 The authors declare that they have no conflict of interest.

645 **Acknowledgement.** We thank Mr. Nguyen Tien Toan at Mid-central Regional Hydro-
646 Meteorological Centre, Viet Nam for kindly providing the observed rainfall and radar data, as well
647 as his comment. We acknowledge the free use of ECMWF ERA5 from Copernicus Climate Change
648 Service (C3S) Climate Data Store (CDS) [https://www.ecmwf.int/en/forecasts/datasets/reanalysis-](https://www.ecmwf.int/en/forecasts/datasets/reanalysis-datasets/era5)
649 [datasets/era5](https://www.ecmwf.int/en/forecasts/datasets/era5). The Vietnam Gridded Precipitation rainfall dataset is available at
650 <http://danida.vnu.edu.vn/cpis/en/content/gridded-precipitation-data-of-vietnam.html>. The TRMM

651 3B42 satellite data are from https://disc.gsfc.nasa.gov/datasets/TRMM_3B42_7/summary. The IR1
652 Himawari imagines data are from Central Weather Bureau, Taiwan at <https://www.cwb.gov.tw>.

653 **References**

654 Akter, N., and Tsuboki, K.: Characteristics of Supercells in the Rainband of Numerically Simulated
655 Cyclone Sidr., SOLA, 6A, 025–028. <https://doi.org/10.2151/sola.6A-007>, 2010.

656 Akter, N., and Tsuboki, K.: Numerical Simulation of Cyclone Sidr Using a Cloud-Resolving Model:
657 Characteristics and Formation Process of an Outer Rainband. Mon. Wea. Rev., 140, 789–810.
658 <http://dx.doi.org/10.1175/2011MWR3643.1>, 2012.

659 Bui, M.T.: Extratropical forcing of submonthly variations of rainfall in Vietnam, J. Climate, 32 (8),
660 2329–2348, 2019.

661 Chen, T.-C., Tsay, J.-D., Yen, M.-C., and Matsumoto, J.: Interannual variation of the late fall rainfall
662 in central Vietnam, J. Climate, 25, 392–413, 2012.

663 Cotton, W.R., Tripoli, G.J., Rauber, R.M., and Mulvihill, E.A.: Numerical simulation of the effects
664 of varying ice crystal nucleation rates and aggregation processes on orographic snowfall. J.
665 Climate Appl. Meteorol. 25, 1658–1680, 1986.

666 Deardorff, J. W.: Stratocumulus-capped mixed layers derived from a three-dimensional model,
667 Bound.-Lay. Meteorol., 18, 495–527, 1980.

668 Huffman, G.J., D.T. Bolvin, E.J. Nelkin, and R.F. Adler.: TRMM (TMPA) Precipitation L3 1 day
669 0.25 degree x 0.25 degree V7, Edited by Andrey Savtchenko, Goddard Earth Sciences Data and
670 Information Services Center (GES DISC), Accessed on 10-12-2019,
671 10.5067/TRMM/TMPA/DAY/7, 2016.

672 Hersbach, H., Bell, B., Berrisford, P., Biavati, G., Horányi, A., Muñoz Sabater, J., Nicolas, J., Peubey,
673 C., Radu, R., Rozum, I., Schepers, D., Simmons, A., Soci, C., Dee, D., and Thépaut, J-N.: ERA5

674 hourly data on pressure levels from 1979 to present. Copernicus Climate Change Service (C3S)
675 Climate Data Store (CDS). (Accessed on 14-06-2021). Doi: 10.24381/cds.bd0915c6, 2018b.

676 Hersbach, H., Bell, B., Berrisford, P., Biavati, G., Horányi, A., Muñoz Sabater, J., Nicolas, J., Peubey,
677 C., Radu, R., Rozum, I., Schepers, D., Simmons, A., Soci, C., Dee, D., and Thépaut, J-N.: ERA5
678 hourly data on single levels from 1979 to present. Copernicus Climate Change Service (C3S)
679 Climate Data Store (CDS). (Accessed on 14-06-2021). DOI: 10.24381/cds.adbb2d47, 2018a.

680 Ikawa, M., and Saito, K.: Description of a non-hydrostatic model developed at the Forecast Research
681 Department of the MRI, MRI Technical report 28, Japan Meteorological Agency, Tsukuba,
682 Japan, 1991.

683 Kondo, J.: Heat balance of the China Sea during the air mass transformation experiment, J. Meteorol.
684 Soc. Jpn., 54, 382–398, https://doi.org/10.2151/jmsj1965.54.6_382, 1976.

685 Lin, Y.-L., Farley, R.D., and Orville, H.D.: Bulk parameterization of the snow field in a cloud model.
686 J. Climate Appl. Meteorol. 22, 1065–1092, 1983.

687 Louis, J. F., Tiedtke, M., and Geleyn, J. F.: A short history of the operational PBL parameterization
688 at ECMWF, in: Proceedings of Workshop on Planetary Boundary Layer Parameterization, 25–
689 27 November 1981, Shinfield Park, Reading, UK, 59–79, 1982.

690 Murakami, M.: Numerical modeling of dynamical and microphysical evolution of an isolated
691 convective cloud – the 19 July 1981 CCOPE cloud, J. Meteorol. Soc. Jpn., 68, 107–128, 1990.

692 Murakami, M., Clark. T.L., and Hall, W.D.: Numerical simulations of convective snow clouds over
693 the Sea of Japan: Two-dimensional simulation of mixed layer development and convective
694 snow cloud formation, J. Meteorol. Soc. Jpn. 72, 43–62, 1994.

695 Nguyen-Le, D., and Matsumoto, J.: Delayed withdrawal of the autumn rainy season over central
696 Vietnam in recent decades. Int. J. Climatol., 36, 3002–3019, 2016.

697 Nguyen-Thi, H.A., Matsumoto, J., Ngo-Duc, T., and Endo, N.: Long-term trends in tropical cyclone
698 rainfall in Vietnam. *J. Agrofor. Environ.*, 6(2), 89–92, 2012.

699 Nguyen-Xuan, T., Ngo-Duc, T., Kamimura, H., Trinh-Tuan, L., Matsumoto, J., Inoue, T., and Phan-
700 Van, T.: The Vietnam Gridded Precipitation (VnGP) Dataset: Construction and validation.
701 SOLA, 12, 291–296, <https://doi.org/10.2151/sola.2016-057>, 2016.

702 Ohigashi, T., and Tsuboki, K.: Shift and intensification processes of the Japan-Sea Polar-Airmass
703 Convergence Zone associated with the passage of a mid-tropospheric cold core. *Journal of the*
704 *Meteorological Society of Japan*, 85(5), 633–662, 2007.

705 ~~705 Roberts, N.M., and Lean, H.W.: Scale selective verification of rainfall accumulations from high-
706 resolution forecasts of convective events. *Mon. Wea. Rev.*, 136, 78–97, 2008.~~

707 ~~707 Segami, A., Kurihara, K., Nakamura, H., Ueno, M., Takano, I., and Tatsumi, Y.: Operational
708 mesoscale weather prediction with Japan Spectral Model. *J. Meteorol. Soc. Jpn.*, 67, 907–924,
709 https://doi.org/10.2151/jmsj1965.67.5_907, 1989.~~

710 Tran, T., Coauthors: The Climate Change and Sea Level Rise Scenarios for Viet Nam. The Ministry
711 of Natural Resources and Environment. Page count:170, 2016.

712 Tsuboki, K., and Sakakibara, A.: Large-Scale Parallel Computing of Cloud Resolving Storm
713 Simulator. In: Zima H.P., Joe K., Sato M., Seo Y., Shimasaki M. (eds) *High Performance*
714 *Computing. ISHPC 2002. Lecture Notes in Computer Science*. Springer, Berlin, Heidelberg.
715 Vol 2327, https://doi.org/10.1007/3-540-47847-7_21, 2002.

716 Tsuboki, K., and Sakakibara, A.: CReSS User's Guide (17th IHP training course text). Page count:
717 273, 2007.

718 Takahashi, H.G., Yoshikane, T., Hara, M., and Yasunari, T.: High-resolution regional climate
719 simulations of the longterm decrease in September rainfall over Indochina. *Atmos. Sci. Let.*, 10,
720 14–18, doi:10.1002/asl.203, 2009.

721 Vu, V.T., Nguyen, T.H., Nguyen, V.T., Nguyen, V.H., Pham, T.T.H., and Nguyen, T.L.: Effects of
722 ENSO on Autumn Rainfall in Central Vietnam. *Advances in Meteorology*, Vol. 2015, Article
723 ID 264373, 12 pages. <http://dx.doi.org/10.1155/2015/264373>, 2015.

724 van der Linden, R., Fink, A.H., Phan-Van, T., and Trinh-Tuan, L.: Synoptic-dynamic analysis of early
725 dry-season rainfall events in the Vietnamese central highlands. *Mon. Wea. Rev.*, 144, 1509–
726 1527. <https://doi.org/10.1175/MWR-D-15-0265.1>, 2016.

727 Wilks, D.S.: *Statistical Methods in the Atmospheric Sciences*, Academic Press. Page count: 648.

728 Wang, C.-C., Lin, B.-X., Chen, C.-T., Lo, S.-H.: [2015](#). Quantifying the effects of long-term climate
729 change on tropical cyclone rainfall using cloud-resolving models: Examples of two landfall
730 typhoons in Taiwan, *J. Climate*, 28, 66–85. <https://doi.org/10.1175/JCLI-D-14-00044.1>, 20[0615](#).

731 Wu, P., Fukutomi, Y., and Matsumoto, J.: The impact of intraseasonal oscillations in the tropical
732 atmosphere on the formation of extreme central Vietnam precipitation. *SOLA*, 8, 57–60.
733 <https://doi.org/10.2151/sola.2012-015>, 2012.

734 Wang, C. G., Liang, J., and Hodges, K. I.: Projections of tropical cyclones affecting Vietnam under
735 climate change: Downscaled HadGEM2-ES using PRECIS 2.1, *Quart. J. Roy. Meteor. Soc.*, 143,
736 1844–1859, <https://doi.org/10.1002/qj.3046>, 2017.

737 Wang, C.-C., Tsai, C.-H., Jou, B.J.-D., and David, S.J.: [Time-Lagged Ensemble Quantitative
738 Precipitation Forecasts for Three Landfalling Typhoons in the Philippines Using the CReSS
739 Model, Part I: Description and Verification against Rain-Gauge Observations. Atmosphere](#), 13,
740 1193. <https://doi.org/10.3390/atmos13081193>, 2022.

741 Yokoi, S., and Matsumoto, J.: Collaborative effects of cold surge and tropical depression-type
742 disturbance on heavy rainfall in central Vietnam, *Mon. Wea. Rev.*, 136, 3275–3287.
743 <https://doi.org/10.1175/2008MWR2456.1>, 2008.

Field Code Changed

744 Yen, M.C., Chen, T.-C., Hu, H.-L., Tzeng, R.-Y., Dinh, D.T., Nguyen, T.T.T., and Wong, C.J.:
745 Interannual variation of the fall rainfall in Central Vietnam, J. Meteor. Soc. Japan, 89A, 259-270.
746 <https://doi.org/10.2151/jmsj.2011-A16>, 2010.

747 Yamada, H., Geng, B., Uyeda, H., and Tsuboky, K.: Role of the Heated Landmass on the Evolution
748 and Duration of a Heavy Rain Episode over a Meiyu-Baiu Frontal Zone, Journal of the
749 Meteorological Society of Japan, Vol. 85, No. 5, 687-709, 2007.

750 Website:

751 Tuoi Tre news (2018) <https://tuoitre.vn/mien-trung-tiep-tuc-mua-lon-14-nguoi-chet-va-mat-tich-201812201907413.htm>

753 Communist Party of Vietnam Online Newspaper (2018) <https://dangcongsan.vn/xa-hoi/mua-lon-tai-mien-trung-la-bieu-hien-ro-ret-cua-bien-doi-khi-hau--507626.html>

Formatted: Font color: Green